Role of aperiodic order in the spectral, localization, and scaling properties of plasmon modes for the design of nanoparticle arrays

Carlo Forestiere,[1] Giovanni Miano,[1] Gugliemo Rubinacci,[1] and Luca Dal Negro[2,3]
[1]*Department of Electrical Engineering, Università degli Studi di Napoli Federico II, Napoli, 80125, italy*
[2]*Department of Electrical and Computer Engineering, Boston University, Boston, Massachusetts 02215, USA*
[3]*Division of Materials Science and Engineering, Boston University, Boston, Massachusetts 02215, USA*
(Received 17 June 2008; revised manuscript received 31 October 2008; published 3 February 2009)

In this paper, we propose a general and efficient method to analyze the dipolar modes of aperiodic arrays of metal nanoparticles with ellipsoidal shapes and their electromagnetic coupling with external fields. We reduce the study of the spectral and localization properties of dipolar modes to the understanding of the spectral properties of an operator L expressing the electric field along the chain in terms of the electric-dipole moments within the electric quasistatic approximation. We show that, in general, the spectral properties of the L operator are at the origin of the formation of pseudoband gaps and localized modes in aperiodic chains. These modal properties are therefore uniquely determined by the aperiodic geometry of the arrays for a given shape of the nanoparticles. The proposed method, which can be easily extended in order to incorporate retardation effects and higher multipolar orders, explains in very clear terms the role of aperiodicity in the particle arrangement, the effect of particle shapes, incoming field polarization, material dispersion, and optical losses. Our method is applied to the simple case of linear arrays generated according to the Fibonacci sequence, which is the chief example of deterministic quasiperiodic order. The conditions for the resonant excitation of dipolar modes in Fibonacci chains are systematically investigated. In particular, we study the scaling of localized dipolar modes, the enhancement of near fields, and the formation of Fibonacci pseudodispersion diagrams for chains with different interparticle separations and particle numbers. Far-field scattering cross sections are also discussed in detail. All results are compared with the well-known case of periodic linear chains of metal nanoparticles, which can be derived as a special application of our general model. Our theory enables the quantitative and predictive understanding of band-gap positions, field enhancement, scattering, and localization properties of aperiodic arrays of resonant nanoparticles in terms of their geometry. This is central to the design of metallic resonant arrays that, when excited by an external electromagnetic wave, manifest strongly localized and enhanced near fields.

DOI: 10.1103/PhysRevB.79.085404 PACS number(s): 73.20.Mf, 42.25.Bs, 42.70.Qs, 42.25.Fx

I. INTRODUCTION

The understanding and the design of optical interactions in deterministic structures without translational invariance offer a vastly unexplored potential for the creation and control of highly localized field states. Unlike periodically arranged photonic crystal structures, deterministic aperiodic structures (DAS) manifest unique light localization and transport properties associated to the multifractal character of their spatial Fourier spectra.[1–4] Unlike random media, deterministic aperiodic structures are defined by simple mathematical rules rooted in symbolic dynamics[2,5–8] and finite inflation rules,[9] which encode a fascinating complexity. Aperiodic dielectric structures share distinctive physical properties with both periodic media, i.e., the formation of large energy gaps, and disordered random media, i.e., the presence of highly localized states characterized by high-field enhancement and anomalous transport properties.[9–13]

In the context of metal plasmonic nanostructures, the study of DAS is still in its infancy. In particular, the understanding of electromagnetic and plasmon coupling in large nanoparticle arrays without translational invariance provides significant challenges to the numerical solution methods of classical electrodynamics. Therefore, in order to fully explore the potential of aperiodic plasmonics for the design and the demonstration of optical devices, there is currently a strong need to formulate simple analytical methods that are able to accurately describe the complex spectral properties of aperiodic and fractal media at reduced computational costs. In particular, the accurate control of electromagnetic coupling and mode localization in deterministic aperiodic metal nanostructures is appealing to a variety of nanodevice applications in the growing areas of field-enhanced nanosensors, engineered surface-enhanced Raman scattering (SERS) substrates, and optical nanoantenna arrays.

The spectral, localization, and dispersion properties of dipolar modes in a Fibonacci linear chain of lossless spherical nanoparticles have been studied in Ref. 14 by using a simple matrix approach based on the electric quasistatic point-dipole approximation. A simple Drude-type model has been used to describe the optical response of the metal. Two-dimensional deterministic aperiodic arrays of plasmonic nanoparticles have also been recently discussed within a coupled dipole approach,[15] and distinctive scattering resonances have been experimentally demonstrated and described using generalized Mie theory.[16]

In this paper, we propose a simple, general, and efficient approach, based on the quasistatic point-dipole approximation, for analyzing both the dipolar modes in quasiperiodic arrays of metal nanoparticles with general ellipsoidal shapes and their coupling with an external electric field. The optical response of the metal is described by its actual dielectric

function, without the need of simplified analytical models. The proposed approach has several significant advantages: (i) a single calculation yields the frequencies and eigenmodes of any aperiodic chain; (ii) particles with ellipsoidal shape, dielectric functions of any form, and the coupling with an external electric field can be considered; (iii) it clearly establishes and separates the respective roles of the dielectric response of the metal, optical losses, dipole polarization, particle shapes, and geometrical arrangement of the particles. Indeed, the governing equations of our model have been formulated in such a way as to separate the effects of the material dispersion, particle shapes, and field polarizations from the geometrical arrangement of the nanoparticles. This allows the complete understanding of the connection between the aperiodic geometry of nanoparticles arrays, and the resulting spectral and modal properties. The approach enables the predictive design of band-gap frequencies, field enhancement, and scattering properties of aperiodic arrays of resonant nanoparticles.

In addition, the possibility to investigate the coupling with an external electric field is very important in order to excite a mode or a dipole distribution of interest by applying an external source. The understanding of the role of the geometrical particle arrangement, polarization, shape, dielectric response, and optical losses is central to the design of metallic resonant arrays that, when excited by an external electromagnetic wave, manifest strongly localized and enhanced near fields.

This paper is organized as follows. In Sec. II we formulate the equations governing the dynamics of the electric-dipole moments of metallic nanoparticle arrays, in the frequency domain, by using the electric quasistatic approximation. In Sec. III we outline the approach that we propose for studying dipolar modes in a general nanoparticle array and we discuss the coupling with an external electric field. In Sec. IV we restrict our general approach to the very interesting case of linear arrays of metal nanoparticles. In Sec. V we apply our method to the study of the dipolar modes in a linear array generated according to the quasiperiodic Fibonacci sequence, which is the most extensively investigated example of a quasiperiodic structure. In Sec. VI we summarize our findings and draw our conclusions.

II. MODEL

In this section we will introduce our general model for the description of dipolar modes and external field coupling in metal nanoparticle arrays. The particles are considered all equal and with ellipsoidal shapes. The axes of the ellipsoids are all oriented along the same direction.

We describe the collective response of the array by modeling each particle as a point-electric dipole (e.g., Refs. 17–19) and considering only the quasistatic contribution to the electromagnetic interaction between the dipoles (e.g., Refs. 14 and 20). We have verified that these assumptions are valid as long as the interparticle separation is at least equal to the characteristic linear dimension of the particles and much smaller compared with the characteristic wavelength of the electromagnetic field.[21]

Let us introduce a rectangular coordinate system (O,x,y,z). The fundamental directions $\hat{\mathbf{x}},\hat{\mathbf{y}},\hat{\mathbf{z}}$ are chosen to be coincident with the three principal axes of the ellipsoids in such a way that their half lengths a_x,a_y,a_z verify the inequality $a_x \leq a_y \leq a_z$. The position vectors of the centers of the ellipsoids are indicated by $\mathbf{r}_1,\mathbf{r}_2,\ldots,\mathbf{r}_N$, where N denotes the number of particles. We indicate with $\mathbf{p}_h$ the electric-dipole moment of the h-th particle and with $\mathbf{E}_h$ the electric-field value at its center generated by all the particles and external sources, in the frequency domain. The relation

$$\mathbf{p}_h = V_0(\varepsilon - \varepsilon_0)\mathbf{E}_h \tag{1}$$

describes the response of the h-th particle to the total electric field $\mathbf{E}_h$; $\varepsilon=\varepsilon(\omega)$ is the dielectric constant of the metal, ε_0 is the vacuum dielectric constant, and $V_0=4\pi a_x a_y a_z/3$ is the particle volume.

The effects of the losses due to the radiation of each nanoparticle may be easily incorporated into the dielectric constant ε for those frequency ranges in which the electromagnetic response of the materials can be described by classical theories as, for example, the Drude model, (e.g., Ref. 22). In this case, we would add to the electron relaxation frequency (due to interactions with phonons, electrons, lattice defects, and impurities) a dissipation term $\Gamma\omega^2/\omega_0^2$, where Γ is the relaxation frequency due to the radiation into the far field and ω_0 is the plasmon frequency of the nanoparticle without including radiation.[23]

The value of the electric field at the h-th particle center generated by the h-th particle itself $\mathbf{E}_{hh}$ is

$$\mathbf{E}_{hh} = -\frac{1}{V_0\varepsilon_0}A\mathbf{p}_h, \tag{2}$$

where $A=\mathrm{diag}(A_x,A_y,A_z)$ is the diagonal dyad of depolarizing coefficients A_x,A_y,A_z whose expressions are given in Appendix A. For a sphere we have $A_x=A_y=A_z=1/3$, for a *prolate* spheroid such that $a_x=a_y$ (cigar shaped) we have $A_x=A_y<A_z$, and for an oblate spheroid such that $a_y=a_z$ (pancake shaped) we have $A_x<A_y=A_z$.

The value of the electric field generated by the k-th particle at the center of the h-th particle, with $h\neq k$, is given by

$$\mathbf{E}_{hk} = \frac{1}{4\pi\varepsilon_0}\frac{1}{r_{hk}^3}B_{hk}\mathbf{p}_k, \tag{3}$$

where $\mathbf{r}_{hk}=(\mathbf{r}_h-\mathbf{r}_k)$, $r_{hk}=|\mathbf{r}_{hk}|$, $\hat{\mathbf{r}}_{hk}=\mathbf{r}_{hk}/r_{hk}$, B_{hk} is the dyad defined as

$$B_{hk} = 3\hat{\mathbf{r}}_{hk}\hat{\mathbf{r}}_{hk} - I, \tag{4}$$

and I is the identity dyad. All the dyads B_{hk} are symmetric.

In conclusion the value of the total electric field at the center of the h-th particle generated by all the particles and the external sources is given by

$$\mathbf{E}_h = -\frac{1}{V_0\varepsilon_0}A\mathbf{p}_h + \frac{1}{4\pi\varepsilon_0}\sum_{\substack{k=1\\k\neq h}}^{N}\frac{1}{r_{hk}^3}B_{hk}\mathbf{p}_k + \mathbf{E}_{\mathrm{ext}}(\mathbf{r}_h), \tag{5}$$

where $\mathbf{E}_{\mathrm{ext}}=\mathbf{E}_{\mathrm{ext}}(\mathbf{r})$ is the electric field due to the external sources. By combining Eqs. (1) and (5) we obtain the system

of linear algebraic equations governing the dipole moments $\mathbf{p}_1, \mathbf{p}_2, \ldots, \mathbf{p}_N$:

$$\frac{\mathbf{p}_h}{V_0(\varepsilon - \varepsilon_0)} = -\frac{1}{V_0\varepsilon_0} A\mathbf{p}_h + \frac{1}{4\pi\varepsilon_0} \sum_{\substack{k=1 \\ k\neq h}}^{N} \frac{1}{r_{hk}^3} B_{hk}\mathbf{p}_k + \mathbf{E}_{\text{ext}}(\mathbf{r}_h) \quad \text{for} \quad h = 1,2, \ldots N. \tag{6}$$

III. COMPUTATIONAL METHOD

In this section we shall introduce, starting from the system of Eq. (6), the computational method that we have developed to study the dipolar modes of metal nanoparticle arrays and their coupling with the external electric field.

It is useful to rewrite the system of Eq. (6) as

$$\alpha(\omega)\mathbf{p}_h + \left[A\mathbf{p}_h - \frac{1}{3}\left(\frac{r_c}{d_c}\right)^3 \sum_{\substack{k=1 \\ k\neq h}}^{N} \left(\frac{d_c}{r_{hk}}\right)^3 B_{hk}\mathbf{p}_k \right] = V_0\varepsilon_0 \mathbf{E}_{\text{ext}}(\mathbf{r}_h) \quad \text{for} \quad h = 1,N, \tag{7}$$

where r_c is the radius of a sphere with the same volume of the ellipsoid, d_c is the minimum distance between the centers of two adjacent nanoparticles, and

$$\alpha = \frac{\varepsilon_0}{\varepsilon(\omega) - \varepsilon_0}. \tag{8}$$

Note that the terms in the square brackets on the left-hand side of Eq. (7) do not depend explicitly on the frequency: the first term inside the brackets only depends on the particle shape while the second one only depends on the geometrical arrangement of the particles in the array.

The vector $\mathbf{p}_h \in C^3$ is the electric-dipole moment of the h-th particle. Now we introduce the array vector $\underline{\mathbf{p}} \in C^{3N}$ that represents the collection of the electric-dipole moments. The equation governing the collection $\underline{\mathbf{p}}$ is

$$[\alpha(\omega)I + L]\underline{\mathbf{p}} = \varepsilon_0 E_0 V_0 \underline{\mathbf{b}}, \tag{9}$$

where I is the identity matrix of order $3N$, $\underline{\mathbf{b}} \in C^{3N}$ represents the forcing term

$$\underline{\mathbf{b}} = \frac{1}{E_0} \begin{vmatrix} \mathbf{E}_{\text{ext}}(\mathbf{r}_1) \\ \mathbf{E}_{\text{ext}}(\mathbf{r}_2) \\ \cdots \\ \mathbf{E}_{\text{ext}}(\mathbf{r}_N) \end{vmatrix}, \tag{10}$$

E_0 is the maximum of the intensity of the external field, and L is a $3N \times 3N$ matrix that can be partitioned into N^2 3×3 blocks L_{hk}. The diagonal blocks L_{hh} are equal and are given by

$$L_{hh} = A. \tag{11}$$

The generic off diagonal block L_{hk} is given by $(h \neq k)$

$$L_{hk} = -\frac{1}{3}\left(\frac{r_c}{d_c}\right)^3 \left(\frac{d_c}{r_{hk}}\right)^3 B_{hk}. \tag{12}$$

The physical meaning of the matrix L is the following: the $3i+1$, $3i+2$, $3i+3$-th elements of the vector $-L\underline{\mathbf{p}}/V_0\varepsilon_0$, with $i=0,1,\ldots,N-1$, are, respectively, the values of the x,y,z components of the intensity of the electric field at the center of the $(i+1)$-th particle, generated by the dipole collection $\underline{\mathbf{p}}$. The quadratic form

$$W = \frac{1}{2\varepsilon_0 V_0} \underline{\mathbf{p}}^T L \underline{\mathbf{p}} \tag{13}$$

represents the energy of the electric field generated by the dipole collection; hence the matrix L is strictly definite positive. Furthermore, it is easy to verify that L is symmetric, as well.

By summarizing, Eq. (9) governs the dipole mode distribution induced by external electromagnetic fields along nanoparticle chains. It has been formulated in such a way as to clearly separate the contribution due to the material properties from those due to the shapes and spatial distribution (geometry) of the nanoparticle arrays. The diagonal blocks of the matrix only depend on the shape while the off diagonal blocks only depend on the positions of the particles. The material properties only enter through $\alpha(\omega)I$.

A. Mode analysis

In this section, we will derive the fundamental connection between the geometry of the arrays and their spectral properties. In particular, we will demonstrate that the eigenvalues and eigenvectors of the operator L are uniquely determined by the arrangement of the nanoparticles in the array for a given shape of the nanoparticles.

The dipolar modes of the nanoparticle array are the solutions of the homogeneous matrix equation:

$$[\alpha(s)I + L]\underline{\mathbf{w}} = \underline{\mathbf{0}}. \tag{14}$$

Therefore, the dipole mode $\underline{\mathbf{w}}_m$ is an eigenvector of the matrix L and the corresponding natural frequencies $s_m = \omega_m + i\mu_m$ are the solutions of the equation:

$$\varepsilon(s_m) = \varepsilon_0\left(1 - \frac{1}{\lambda_m}\right), \tag{15}$$

where λ_m is the eigenvalue of L associated to the eigenvector $\underline{\mathbf{w}}_m$. From the study of the spectral properties of the matrix L, we shall obtain the main properties of the dipole modes of the array. Interestingly we notice that, within the dipolar approximation used here, the dipole modes only depend on the shape of the particles and their geometrical arrangement.

Let us consider now the eigenvalue problem:

$$L\underline{\mathbf{w}} = \lambda\underline{\mathbf{w}}. \tag{16}$$

Since the matrix L is symmetric, all its eigenvalues and the corresponding eigenvectors are real and the eigenvectors are orthogonal; in addition, since the matrix L is strictly definite positive all the eigenvalues are positive. Furthermore, as we shall see later, all the eigenvalues are less than one, thus $0 < \lambda < 1$. As a consequence, the eigenfrequencies exist only in the intervals of frequency where the real part of the dielectric constant is negative. We normalize the eigenvectors in such a way that

$$\underline{\mathbf{w}}_m^T \underline{\mathbf{w}}_n = \delta_{mn} \quad \text{for} \quad m,n = 1,2,\ldots,3N, \tag{17}$$

where δ_{mn} is the Kronecker symbol and order the eigenvalues in such a way $\lambda_1 \leq \lambda_2 \leq \ldots \leq \lambda_{3N}$.

To solve Eq. (15) we need to know the analytical continuation of $\varepsilon(\omega)$ to the entire complex plane $s=\omega+i\mu$. In general, we do not have an analytical expression for $\varepsilon(\omega)$ but only a discrete set of values for its real and imaginary parts in the frequency range of interest, as experimentally measured. Nevertheless, it is always possible to approximate adequately $\varepsilon(\omega)$ through rational functions starting from the measured data by using standard identification techniques. Once this approximation has been found, its analytical continuation to the entire complex plane is immediately obtained by replacing ω with s. In this way the solution of Eq. (15) is reduced to the solution of an algebraic equation with complex coefficients. For frequency ranges in which the electromagnetic response of the material is well described by classical models such as, for example, the Drude model (e.g., Ref. 22), the expression of $\varepsilon(\omega)$ is known analytically and the solution of Eq. (15) becomes straightforward. The expression of the dielectric constant based on the Drude model is

$$\varepsilon(\omega) = \varepsilon_0 \left[1 - \frac{\omega_p^2}{\omega(\omega - i\nu)} \right]. \tag{18}$$

where ω_p is the plasma frequency of the free electrons of the metal and ν is the relaxation frequency due to interactions with phonons, electrons, lattice defects, and impurities. By solving Eq. (15) we obtain

$$\omega_m = \omega_p \sqrt{\lambda_m - \left(\frac{\nu}{2\omega_p} \right)^2}, \tag{19}$$

$$\mu_m = \frac{\nu}{2}. \tag{20}$$

Being $\nu/\omega_p \ll 1$, for $\lambda_m = O(1)$ from expression (19) we obtain

$$\omega_m \cong \omega_p \sqrt{\lambda_m} \left[1 - \frac{1}{2\lambda_m} \left(\frac{\nu}{2\omega_p} \right)^2 \right] \tag{21}$$

By summarizing, the modes of the nanoparticle chain, which are real and orthogonal, are all the eigenvectors of the matrix L; thus they only depend on the particle shapes and their geometrical arrangements. On the other hand, as shown in Eq. (21), the natural frequencies of these eigenmodes depend on the metal response, and they are the solutions of the algebraic Eq. (15). Due to the presence of metal losses, which brings an extra damping factor into Eq. (21), the dipolar modes decay exponentially in time. This damping induces an additional redshift of the system's eigenfrequencies.

B. Coupling with the external electric field

Now we shall study the coupling of plasmonic arrays with the external electric field by using the dipolar modes as basis to represent the dipole distribution along the chain. The solution $\underline{\mathbf{p}}$ of system (9) may be represented through the eigenvectors $\underline{\mathbf{w}}_1, \underline{\mathbf{w}}_2, \ldots, \underline{\mathbf{w}}_{3N}$ of the matrix L:

$$\underline{\mathbf{p}} = \sum_{n=1}^{3N} a_n \underline{\mathbf{w}}_n, \tag{22}$$

where the coefficients $a_1, a_2, \ldots, a_{3N}$ are unknown. Since the eigenvectors are orthonormal, the coefficient a_n is the projection of $\underline{\mathbf{p}}$ along the eigenvector $\underline{\mathbf{w}}_n$,

$$a_n = \underline{\mathbf{w}}_n^T \underline{\mathbf{p}}. \tag{23}$$

By substituting Eq. (22) into Eq. (9), multiplying on the left-hand side by $\underline{\mathbf{w}}_m^T$, and by using Eq. (16), we obtain

$$a_m(\omega) = V_0 \varepsilon_0 E_0 \frac{c_m}{\alpha(\omega) + \lambda_m}, \tag{24}$$

where the coupling coefficient c_m is given by:

$$c_m = \underline{\mathbf{w}}_m^T \underline{\mathbf{b}}. \tag{25}$$

It describes the coupling intensity between the external electric field and the m-th mode.

The external electric field is in resonance with the m-th mode at the frequency Ω_m for which the mode response function,

$$R_m(\omega) = \frac{1}{|\alpha(\omega) + \lambda_m|}, \tag{26}$$

is maximum. Since $0 < \lambda < 1$, the resonance frequencies exist only in the intervals of the frequency where the real part of the dielectric constant is negative.

If $\varepsilon(\omega)$ is experimentally measured, the frequencies for which R_m is maximum may be evaluated numerically. Instead, in the frequency ranges where the electromagnetic response of the material is well described by analytical models such as the Drude model (e.g., Ref. 22), Ω_m may be evaluated analytically. By using the Drude model we obtain the following expression for Ω_{ih}:

$$\Omega_m = \sqrt{\omega_m^2 - \frac{1}{4}\nu^2} = \omega_p \sqrt{\lambda_m - \frac{1}{2}\left(\frac{\nu}{\omega_p} \right)^2}. \tag{27}$$

The 3 dB bandwidth of the response function $R_m(\omega)$ is given by

$$\Delta\Omega_m = \nu \sqrt{1 + \left(\frac{\nu}{2\Omega_m} \right)^2}. \tag{28}$$

Being $\nu/\omega_p \ll 1$ and $\lambda_h : o(1)$ from Eqs. (27) and (28), we obtain, respectively:

$$\Omega_m \cong \omega_p \sqrt{\lambda_m} \left[1 - \frac{1}{4\lambda_m} \left(\frac{\nu}{\omega_p} \right)^2 \right], \tag{29}$$

$$\Delta\Omega_m \cong \nu. \tag{30}$$

In this case the intensity of the m-th mode at the resonance frequency Ω_m is approximately given by

$$a_m(\Omega_m) \cong -iV_0 \varepsilon_0 E_0 \frac{\omega_p}{\nu} \frac{\underline{\mathbf{w}}_m^T \underline{\mathbf{b}}}{\sqrt{\lambda_m}}. \tag{31}$$

By summarizing, the dipole distribution induced along the nanoparticle chain by external electric fields has been repre-

sented through the superposition of the dipolar modes. The amplitude of each dipolar mode depends on three elements: the volume of the particle, the coupling coefficient between the external electric field and the mode, and the response function of the mode. The resonance frequency of the mode is the frequency at which the absolute value of its response function is maximum. Due to the presence of optical losses, the values of the resonance frequencies differ from the values of the natural frequencies. The selectivity of the coupling between the array and an external electric field depends on the 3 dB bandwidth of the mode response functions, and it is limited by the losses and by the dispersion diagram of the eigenvalues λ_m.

IV. APPLICATION TO LINEAR NANOPARTICLE ARRAYS

We now restrict our general results to the very interesting case of linear nanoparticle arrays.[23–27] The array axis coincides with the x axis of the coordinate system. In this case the dyad B_{hk} is given by

$$B_{hk} = \mathrm{diag}(2,-1,-1). \tag{32}$$

Since B_{hk} is diagonal the x components $p_{1x},p_{2x},\ldots,p_{Nx}$, y components $p_{1y},p_{2y},\ldots,p_{Ny}$, and z components $p_{1z},p_{2z},\ldots,p_{Nz}$ of the electric-dipole moments are all uncoupled between them. As consequence, eigenvalue problem (16) further simplifies. Let us denote the longitudinal modes with $\underline{\mathbf{u}}_{\mathbf{P}}=|p_{1x},p_{2x},\ldots,p_{Nx}|^T$ and the transverse ones with $\underline{\mathbf{u}}_{\perp}=|p_{1t},p_{2t},\ldots,p_{Nt}|^T$ with $t=y,z$. All these modes are solutions of the eigenvalue problem:

$$Q\underline{\mathbf{u}} = \beta\underline{\mathbf{u}}, \tag{33}$$

where the element q_{ij} of the $N\mathrm{x}N$ matrix Q is given by

$$q_{ij} = \begin{cases} 0 & \text{for } i=j, \\ \dfrac{d_c^3}{|r_{ij}|^3} & \text{for } i\neq j. \end{cases} \tag{34}$$

Unlike the matrix L, the matrix Q is not definite positive but it is still symmetric; hence it has both positive and negative eigenvalues. The eigenvalues β are ordered in such a way $\beta_1\leq\beta_2\leq\ldots\leq\beta_N$. The corresponding eigenvalues λ_S, with $s=\mathbf{P},\perp$, are given by

$$\lambda_S = A_S + \frac{\eta_S}{3}\left(\frac{r_c}{d_c}\right)^3\beta, \tag{35}$$

where $A_{\mathbf{P}}=A_x$, $A_{\perp}=A_y,A_z$, $\eta_{\mathbf{P}}=-2$, and $\eta_{\perp}=1$. As $r_c/d_c\rightarrow 0$ it results with $\lambda_S\rightarrow A_S$ and the plasmon resonances tend to those of the single particles. The coupling effects give rise to blueshift (redshift) for the transverse modes with $\beta>0$ ($\beta<0$) and vice versa for longitudinal modes. We remark that for the consistency of the model $r_c/d_c\rightarrow 0$ for $A_x=A_y\rightarrow 1/2$, $A_z\rightarrow 0$ (a needle orthogonal to the chain axis) or $A_y=A_z\rightarrow 0$, $A_x\rightarrow 1$ (a disk orthogonal to the chain axis).

By applying the Gerschgorin first theorem[28] to the complete matrix Q, we obtain $|\beta|<2.5$. Since $|\beta|<2.5$ it follows that $0<\lambda_S<1$. The property $0<\lambda_S<1$ is more general,[29] and may be shown by starting from the equation governing the polarization field density in the electroquasistatic approximation.[20]

As we shall see, the components of the eigenvectors corresponding to the highest eigenvalues β vary smoothly if compared with the components of the eigenvectors corresponding to the lowest eigenvalues. As consequences, the characteristic wavelengths of the longitudinal modes decrease as their natural frequencies increase, whereas the characteristic wavelengths of the transverse ones increase.

In the ideal case of lossless metallic nanoparticles, it is always possible to excite a certain mode by choosing the frequency of the external electric field coinciding with the resonance frequency of that mode. In the real case, due to the presence of losses, this possibility depends mainly on three factors: (i) the intensity of the coupling coefficient c_m of the mode with the external electric field, (ii) the bandwidth of the mode response functions $R_m(\omega)$, and (iii) the detuning, in terms of resonance frequency, from the adjacent modes.

The dipole moment distribution induced by an external uniform electric field only depends on $V_0\varepsilon_0E_0$, the polarization of the external electric field, and the following dimensionless groups of physical variables: A_S, ν/ω_p, and r_c/d_c. Let us consider the difference of the resonance frequencies of two adjacent modes $\underline{\mathbf{u}}_q$ and $\underline{\mathbf{u}}_{q+1}$. For $A_S\gg(r_c/d_c)^3$ we have approximately [by using Eq. (27)]:

$$|\Omega_{q+1}-\Omega_q| \cong \omega_p\frac{|\eta_S|}{6\sqrt{A_S}}\left(\frac{r_c}{d_c}\right)^3|\beta_{q+1}-\beta_q|. \tag{36}$$

To improve the selectivity of the nanoparticle chain, we need to increase $(\Omega_{q+1}-\Omega_q)$. This may be obtained both by reducing A_S, increasing $|\eta_S|$, and increasing r_c/d_c. The polarization parameter η_S only assumes two values, -2 and 1 for longitudinal and transverse polarizations, respectively. Since a particle cannot penetrate the nearest ones, the geometrical factors r_c/d_c and A_S are not independent. For spherical particles it results $A_S=1/3$ and $r_c/d_c\leq 1/2$. Actually, we have to impose $r_c/d_c\leq 1/3$ for the validity of the point-dipole approximation.

At this point, we again emphasize that our results, valid within the dipole approximation, demonstrate in clear terms the fundamental connection between the geometry of the arrays and their spectral properties. In fact, we have shown so far that the natural modes and the spectral properties of linear arrays of metallic nanoparticles do not even depend on the shape of the particles and dipole polarization but only depend on the spatial distribution of the particles positions. The particle shape and the dipole polarization only affect the resulting eigenvalues λ in the simple way given by Eq. (35). Furthermore, we have shown that the excitability of single modes through a uniform external electric field is fundamentally limited by optical losses.

V. RESULTS FOR A FIBONACCI LINEAR ARRAY

In this section we apply our general method to the study of Fibonacci arrays of metal nanoparticles, which are the chief example of deterministic aperiodic systems with quasiperiodic Fourier spectrum.[8,14,16,30–35]

TABLE I. The number of particles N of the Fibonacci chain is given for several values of the sequence index j.

j	1	2	3	4	5	6	7	8	9	10	11	12	13	14	15
N	3	4	6	9	14	22	35	56	90	145	234	378	611	988	1598

Differently from the case of periodic structures, aperiodic chains are generated when the distances between adjacent particles are modulated by deterministic aperiodic rules. In Fibonacci linear arrays the set of distance between adjacent particles is composed of two values that we denote with d_A and d_B. Without loss of generality, we shall assume $d_A \leq d_B$. The set of distances is generated by the inflation rule: $A \rightarrow AB$, $B \rightarrow A$. We shall start the Fibonacci sequence with the seed element $F_0=A$, therefore, $F_1=AB$, $F_2=ABA$, $F_3=ABAAB$, etc. The Fibonacci sequences display the property $F_j=\{F_{j-1},F_{j-2}\}$ for $j \geq 2$. In Table I the number of particles N of the Fibonacci chain is given for several values of the sequence index j.

In this paper we restrict our investigation to: (i) the main properties of the dipolar plasmon modes in a linear Fibonacci chain of spherical nanoparticles, $A_S=1/3$, with $r_c/d_A=1/3$; (ii) the coupling of the Fibonacci chain with a uniform external electric field. The behavior of the metal is described through the Drude model by assuming $\nu/\omega_p=10^{-3}$.

The eigenvalues β and eigenvector $\underline{\mathbf{u}}$ of the matrix Q have been conveniently evaluated numerically by using Matlab®. The eigenvalues and eigenvectors of the matrix Q have been compared, respectively, with the eigenvalues and eigenvectors of the matrix obtained by retaining only the nearest-neighbor interactions in the matrix Q. The difference between the eigenvalues and the difference between the eigenvectors may be larger than 20%.

A. Plasmonic resonance frequencies

Here we study the main properties of the resonant frequencies of the plasmonic modes in a Fibonacci linear array. The natural frequencies share the same behavior of the resonant modes because the two are related via Eq. (32).

Expression (27) gives the resonance frequencies of the chain in terms of the eigenvalues λ of the matrix L, the plasma frequency, and relaxation frequency of the metal. The eigenvalues λ are given by Eq. (36) uniquely in terms of the geometrical parameters of the array and of the mode polarization. By combing Eqs. (27) and (36) we obtain for the resonance frequencies Ω_m

$$\Omega_m = \omega_p \sqrt{A_S - \frac{1}{4}\left(\frac{\nu}{\omega_p}\right)^2 + \frac{\eta_S}{3}\left(\frac{r_c}{d_c}\right)^3 \beta_m} \quad \text{for} \quad s = \mathbf{P}, \perp , \tag{37}$$

where $A_{\mathbf{P}}=A_x$, $A_\perp=A_y,A_z$, $\eta_{\mathbf{P}}=-2$, $\eta_\perp=1$, and β_m are the eigenvalues of the matrix Q given by Eq. (35), which only depends on the positions of the nanoparticle centers. Expression (37) clearly highlights the role of the shape, size, and geometrical arrangement of the nanoparticles and the role of the mode polarization. In particular, as we have already emphasized, the resonance frequencies uniquely depend on the geometrical arrangement of the nanoparticles through the eigenvalues β. For this reason we start investigating the general behavior of the eigenvalues β, which are ordered in such a way $\beta_1 \leq \beta_2 \leq \ldots \leq \beta_q \leq \ldots \leq \beta_N$. Here we always refer to a Fibonacci chain with index $j=10$; corresponding to $N=145$.

Figure 1(a) shows the eigenvalue β versus its index q expressed in percentage of the maximum index N for several values of the interdistance ratios d_B/d_A. The eigenvalues β cover almost uniformly the interval $(-1.8031\ldots,2.4040\ldots)$. In the limiting case of $d_B/d_A=1$, the Fibonacci array reduces to a periodic array with equally spaced particles. For $d_B/d_A>1$, plasmonic gaps arise in the eigenvalue curves.[14] For $d_B/d_A=1.25$ the eigenvalue curve shows several gaps. The gaps around $q=34$, $q=55$, $q=89$, and $q=110$ become wider as the ratio d_B/d_A increases. On the opposite, the remaining gaps become narrower and their width reduces to zero with increasing d_B/d_A ratio. Therefore, the plasmon spectral gaps in an aperiodic deterministic array are a direct consequence of the aperiodic geometrical arrangement of the constituent nanoparticles along the chain, and the band-gap positions can be accurately predicted. In order to quantitatively understand the connection of Fibonacci band-gap positions and the arrays geometry, we show in Fig. 1(b) the amplitude of the discrete Fourier transform (DFT) of the Fibonacci sequence $d_A,d_B,d_A,d_A,d_B,d_A,d_B,\ldots$ versus the normalized spatial frequency expressed as $2\pi(N-1)/Nl$, where l denotes the chain length. We can see form Figs. 1(a) and 1(b) that the normalized indexes at which the gaps arise match exactly the normalized frequencies of the spatial Fourier components of the Fibonacci sequence with large amplitudes. It is also evident that the largest gaps correspond to the Fourier components with the highest amplitudes. As d_B/d_A increases, only the gaps corresponding to the spatial Fourier components with the four largest amplitudes remain in the dispersion diagram that reduces to five segments parallel to the horizontal axis. For $d_B/d_A \geq 5$ the eigenvalues β tend to five values -1.353 $(1 \leq q \leq 33)$, -1.000 $(34 \leq q \leq 56)$, -0.125 $(57 \leq q \leq 89)$, $+1.000$ $(90 \leq q \leq 112)$, and $+1.478$ $(113 \leq q \leq 145)$.

This behavior is general, and it is related to the fact that Fibonacci chains are generated according to cube-free and recurrent mathematical sequences.[30,36,37] In the limit $d_B/d_A \rightarrow \infty$, only the four gaps corresponding to the spatial Fourier components with the four largest amplitudes remain in the Fibonacci dispersion diagram. The eigenvalues β exactly assume the five values $-1.353\ldots$, -1.000, -0.125, 1.000, and the system becomes completely degenerate. In the Fibonacci chains with odd indexes the eigenvalues additionally assume the value zero.

Let us now discuss in detail the origin of this degeneracy. In the limit $d_B/d_A \rightarrow \infty$, the array becomes a chain of thee types (one particle, two particles, and three particles) of isolated clusters and the eigenvalue problem can be solved analytically. Indeed, since Fibonacci sequences are cube free,

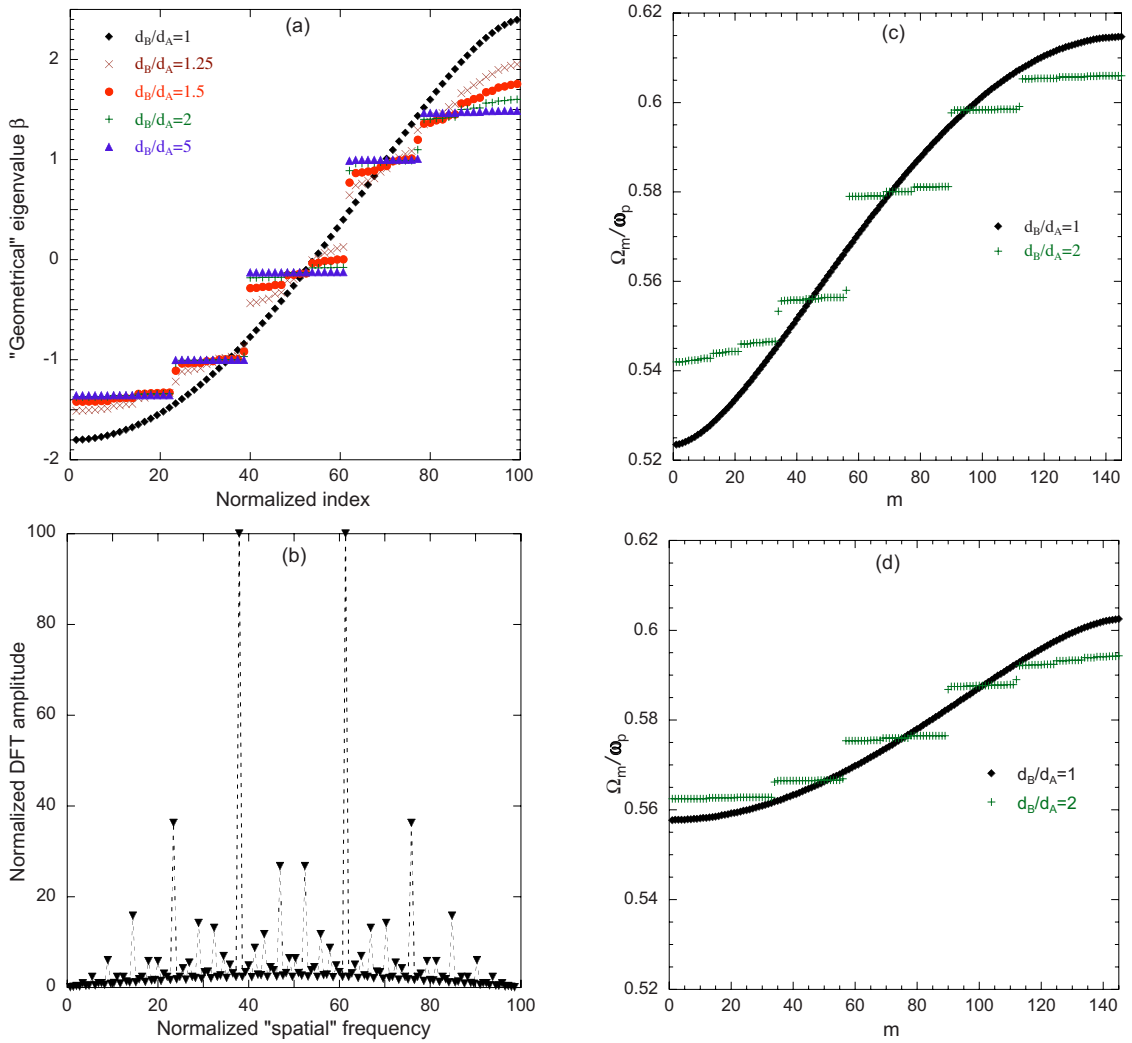

FIG. 1. (Color online) Linear Fibonacci chain with index $j=10$: (a) geometrical eigenvalues β vs normalized index, for ♦ $d_B/d_A=1$, × $d_B/d_A=1.25$, ● $d_B/d_A=1.5$, + $d_B/d_A=2.0$, and ▲ $d_B/d_A=5$; (b) normalized DFT amplitude of the Fibonacci sequence vs normalized "spatial" frequency; resonance frequencies Ω_m of the (c) longitudinal and (d) transverse modes normalized to the plasma frequency ω_p vs modal index m for ♦ $d_B/d_A=1$ and + $d_B/d_A=2.0$.

the symbol A can consecutively occur only one or two times while the symbol B occurs consecutively only once. As a consequence, for $d_B/d_A \to \infty$ we can only have clusters composed of at most one, two, or three particles. The eigenvalue β of a single isolated particle is equal to zero; the eigenvalues β of two interacting nanoparticles are -1 and $+1$; the eigenvalues β of three equally spaced nanoparticles are $(1+3\sqrt{57})/16 \cong 1.478$, -0.25, and $(1-3\sqrt{57})/16 \cong -1.353$. The number of degeneracy of each of them is equal to the number of corresponding clusters in the chain. In addition, since Fibonacci sequences terminates with alternating symbols (A or B) at each generation, in the Fibonacci sequences with odd generation indexes, there is one isolated particle at the end of the chain (cluster B).

Once the eigenvalues β has been evaluated, by using expression (38) we can calculate the resonance frequencies of the plasmon modes. Figures 1(c) and 1(d) show the resonance frequencies Ω_m normalized to the plasmon frequency ω_p versus the modal index m for two different mode polarizations and in the two cases $d_B/d_A=1$ and $d_B/d_A=2$, using $A_S=1/3$, $r_c/d_c=1/3$, and $\nu/\omega_p=10^{-3}$. The resonance frequencies are ordered in such a way that $\Omega_1 \leq \Omega_2 \leq \ldots \leq \Omega_m \leq \ldots \leq \Omega_N$. Since the interaction between the longitudinal modes is stronger than the interaction between the transverse ones,[26] the width of the gaps in the dispersion diagram for the longitudinal modes [Fig. 1(c)] is roughly twice as large compared to the width of the gaps in the dispersion diagram for the transverse modes [Fig. 1(d)]. We emphasize that, in the general case of differently shaped particles of different sizes, the width of the gaps additionally depends on the nanoparticle shapes and sizes as well as the geometric arrangement along the chain. However, this only affects the components of the matrix A and nothing else changes in the formulation of the general problem.

By summarizing, the above results clearly demonstrate that the main properties of the resonance (natural) frequencies of a linear nanoparticle chain may be studied conveniently by analyzing the dispersion diagrams for the eigenvalues β of the matrix Q, which describes the geometrical arrangement of the nanoparticles. We have found a universal

behavior of the dispersion diagram of linear Fibonacci array rooted in the cube-free property of Fibonacci sequences. In particular, we explained the formation of four large gaps at the normalized indexes matching the normalized Fourier components of the Fibonacci sequence with the highest amplitudes. For values of d_B/d_A close to one, plasmonic band gaps open due to the resonant coupling between the modes of an underlying periodic lattice with period d_A and particle number N, and the Fourier components of the Fibonacci array with large amplitudes. For values of d_B/d_A much larger than one, the chain reduces to a set of noninteracting clusters composed of one, two, or three particles. In this case, the system has a strong degeneracy with four or five distinct natural frequencies, depending on the parity of the Fibonacci generation index.

B. Plasmon dipolar modes

Here we study the plasmon dipolar modes of the Fibonacci linear arrays. They are the eigenvectors of the matrix Q defined as in Eq. (34). Therefore, the plasmon dipolar modes of a linear array, unlike their resonance frequencies, only depend on the geometrical arrangement of the nanoparticles in the chain. For the reasons discussed above, we will only consider the longitudinal-mode polarization. The dipolar modes will be ordered according to the order for the resonance frequencies of the longitudinal modes.

The localization character of the plasmon modes is described by the participation ratio defined as[14]

$$P = \frac{1}{N}\frac{\|\underline{\mathbf{u}}\|_2^2}{\|\underline{\mathbf{u}}\|_4^4}. \tag{38}$$

Since the eigenvectors are all normalized so that $\|\underline{\mathbf{u}}\|_2=1$, the participation ratio yields a quantitative measure of the localization degree of the eigenvectors. The eigenmodes with smallest participation ratios are strongly localized.

For $d_B/d_A=1$, the eigenvectors of the matrix Q are the dipolar modes of an aperiodic array with equidistant nanoparticles. The elements of the eigenvector corresponding to the largest eigenvalue β_N are given by the samples of the sine function $\sin[\pi h/(N+1)]$ for $h=1,2,\ldots,N$. Therefore, the modes corresponding to largest eigenvalues β are those with the largest characteristic wavelengths. On the opposite, the modes corresponding to the smallest eigenvalues β are those with the shortest characteristic wavelengths. The participation ratios of the dipolar modes are almost uniform around the value of 0.671. Indeed, the dipolar modes of a periodic linear array are all extended.

As the ratio d_B/d_A increases, the participation ratio decreases and the modes become progressively more localized in different areas of the chain. Figure 2 shows the participation ratio vs the modal index m for (a) $d_B/d_A=1.25$ and (b) $d_B/d_A=2.0$. As the ratio d_B/d_A increases, the participation ratio decreases and becomes strongly oscillating. In particular, the smallest value of the participation ratio, $M \equiv \min_{m\in[1,N]}(P_m)$, decreases as the ratio d_B/d_A increases. Figure 3(a) shows $\log_{10}(M)$ versus d_B/d_A for several values of the Fibonacci generation index. As d_B/d_A varies from 1 to 1.5,

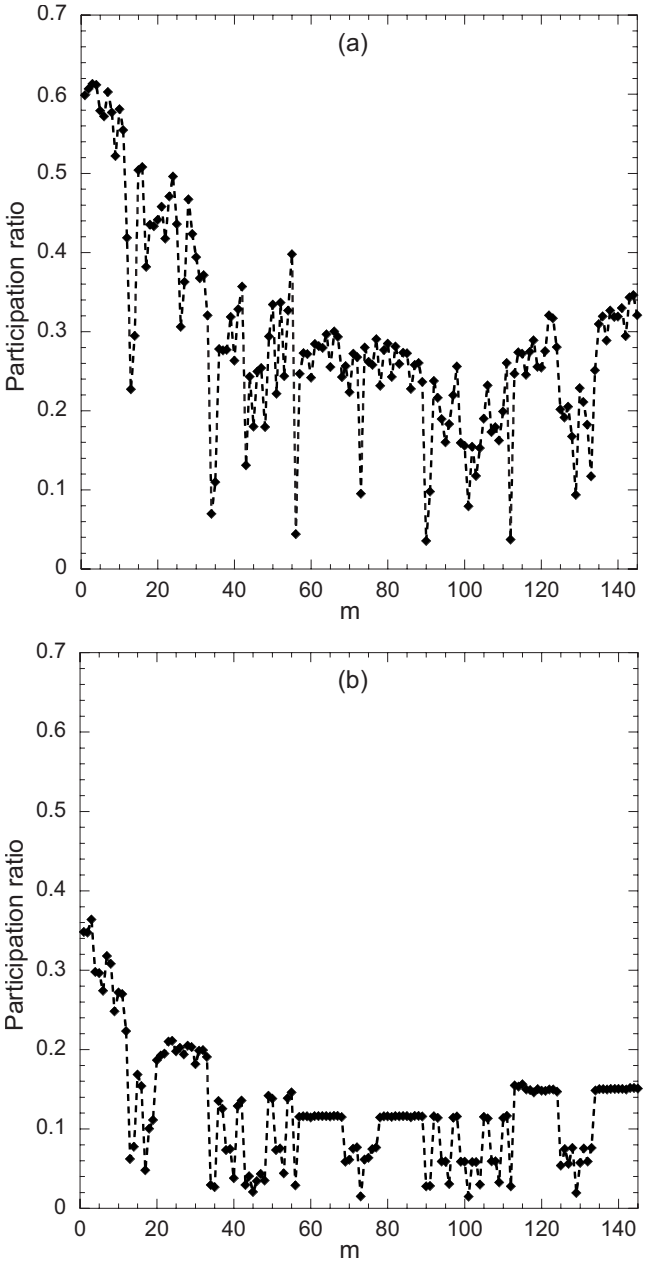

FIG. 2. Linear Fibonacci chain with $j=10$: participation ratio vs the modal index m for (a) $d_B/d_A=1.25$ and (b) $d_B/d_A=2$.

M decreases abruptly by roughly one or two orders of magnitude depending on the Fibonacci index j. For $d_B/d_A>1.5$, M continues to decrease as d_B/d_A increases but more slowly. Therefore, the modes become strongly localized as d_B/d_A moves from one. The participation ratio also varies as the Fibonacci index varies. In Fig. 3(b) we show $R\equiv\ln(M)$ as function of the Fibonacci index j for three values of d_B/d_A. The quantity R decreases as j increases. For large values of d_B/d_A the decrease in R terminates with an oscillation followed by a plateau. As it results from Fig. 3(b) the decrease in R is adequately described by a linear interpolation function $R=c_0-c_1 j$ [Fig. 3(b), full lines]. In Table II the coefficients c_0 and c_1 are given for the three cases. Both the coefficients depend on d_B/d_A. Then the participation ratio decreases as j increases with an exponential scaling law

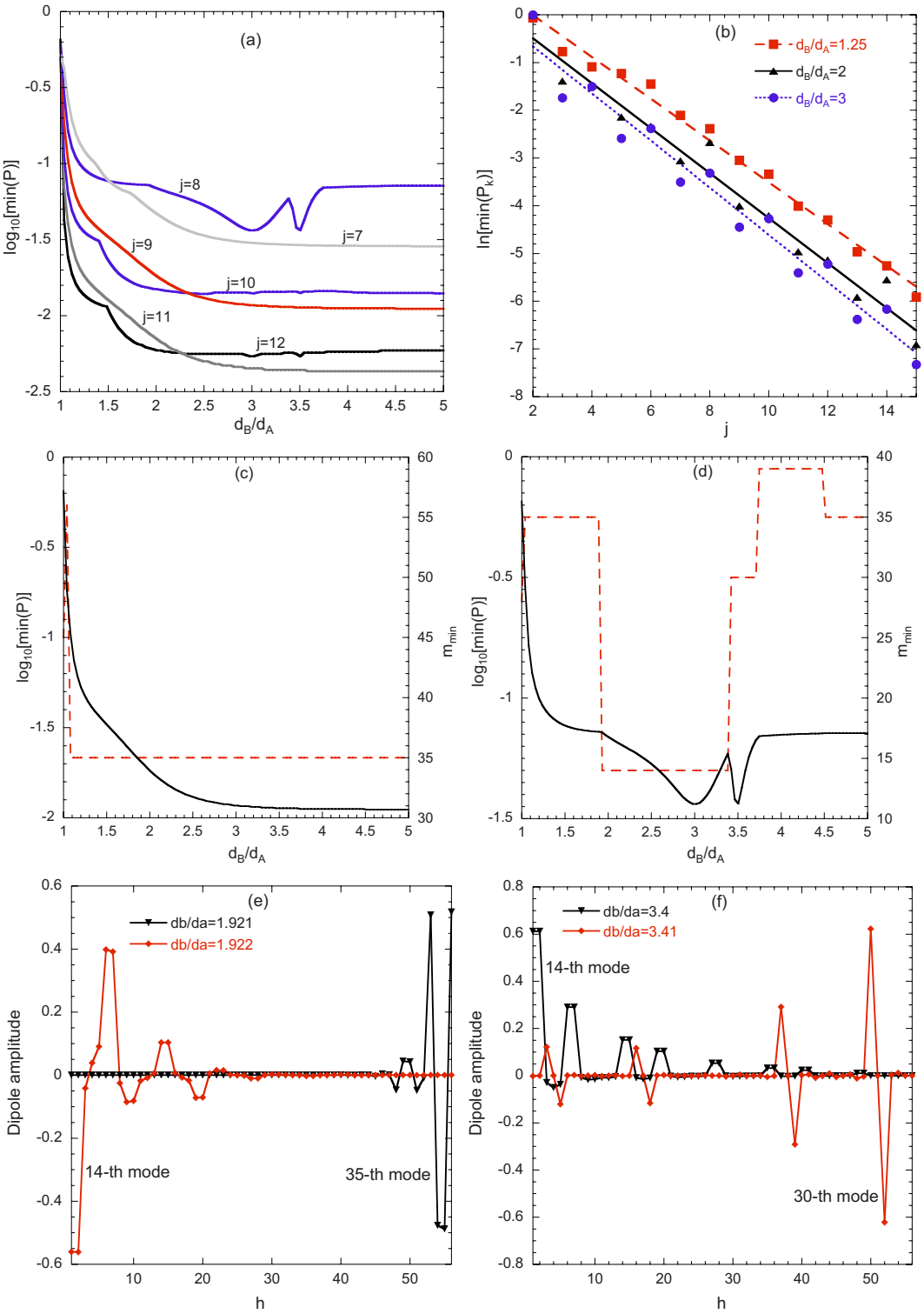

FIG. 3. (Color online) (a) $M=\log_{10}[\min_{m\in[1,N]}(P_m)]$ vs d_B/d_A for several Fibonacci indexes; (b) $\ln[\min_{m\in[1,N]}(P_m)]$ vs Fibonacci index for three values of d_B/d_A; M (full line) and index $m_{\min}$ (dashed line) of the mode with the minimum participation ratio vs d_B/d_A for (c) $j=8$ and (d) $j=9$; [(e) and (f)] some critical modes in the chain with $j=8$.

whose decay constant is given by c_1. As the ratio d_B/d_A increases, the decay constant increases slightly.

Some remarks on the behavior of M as a function of d_B/d_A [Fig. 3(a)] are now appropriate. The behavior of the M functions associated to odd Fibonacci indexes are smooth while those associated to even Fibonacci indexes show pronounced edges and kinks. The origin of this nonmonotonic behavior can simply be understood by the fact that the mode with minimum participation ratio changes abruptly for certain values of the d_B/d_A ratio. This is demonstrated by plot-

TABLE II. The coefficients c_0 and c_1 are given for the three cases. Both the coefficients depend on d_B/d_A.

d_B/d_A	c_0	c_1
1.25	0.86	0.44
2.0	0.45	0.47
3.0	0.32	0.49
5.0	0.28	0.48

ting the index $m_{\min}$ of the mode with the minimum participation ratio as function of d_B/d_A, as shown in Figs. 3(c) and 3(d), and by comparing it with the trend of the function M. When the Fibonacci index is odd $m_{\min}$ only changes for values of d_B/d_A near one while for larger values of d_B/d_A, $m_{\min}$ is constant, as shown in Fig. 3(c). In these chains, the mode with the minimum participation ratio is always localized on the right-hand side for values of d_B/d_A much larger than one because, as already discussed, in these chains there is always a particle well isolated from the others at the right end side (cluster B). On the other hand, when the Fibonacci index is even, $m_{\min}$ oscillates for large values of d_B/d_A because under this condition only clusters with two or three particles can exist [Fig. 3(d)]. Figure 3(e) shows the transition from the 35-th mode to the 14-th mode as d_B/d_A crosses 1.9 and Fig. 3(f) shows the transition from the 14-th to the 30-th mode as d_B/d_A crosses 3.4 in the Fibonacci chain with $j=8$. In the intervals (1.9, 3.4) and (3.4, 3.7) M has local minima at $d_B/d_A \cong 3$ and $d_B/d_A \cong 3.5$ because the 14-th and the 30-th modes are more localized for $d_B/d_A \cong 3$ and $d_B/d_A \cong 3.5$, respectively.

In Fig. 4 we show the spatial distributions of the most localized modes in a Fibonacci linear array with $j=10$. Figures 4(a)–4(c) show the distributions of the 34-th mode, corresponding to the longitudinal resonance frequency $\Omega_{34} \cong 0.553\omega_p$, for $d_B/d_A=1$, $d_B/d_A=1.25$, and $d_B/d_A=2.0$. Figures 4(d)–4(f) show the distributions of the 73-th mode, corresponding to the longitudinal resonance frequency $\Omega_{73} \cong 0.580\omega_p$, for the same values of d_B/d_A. In both cases, the modes become strongly localized as d_B/d_A increases according to the behavior of the participation ratio shown in Fig. 2. Both the modes in the periodic limit are extended along the chain.

The plasmonic band gaps which open in the Fibonacci chains can be completely understood by studying the pseudodispersion diagrams of the modes,[14,38] as shown in Fig. 5 for the longitudinal polarized modes and several values of d_B/d_A. The natural frequencies of the modes, normalized to the plasma frequency, are represented on the ordinate axis while wave numbers K, normalized to π/l, are represented on the abscissa axis. The intensity of the Fourier components of each Fibonacci mode, calculated by the Fourier transform of the eigenvectors, is represented on a black–white intensity scale. Figure 5(a) shows the well-known dispersion curve of the longitudinal plasmon modes in a periodic array. As d_B/d_A deviates from one, the dispersion curve breaks into several Fibonacci pseudogaps, as shown in Figs. 5(b) and 5(c). As d_B/d_A increases even further, the gaps widen until the branches of the dispersion curve reduce to a set of five segments parallel to the wave vector axis, as shown in Figs. 5(d)–5(f). The branches of the pseudodispersion curves show positive slopes since the eigenvalues β of the modes with the largest spatial frequencies and the polarization parameter $\eta_{\mathbf{P}}$ are negative. The pseudodispersion diagram of the transverse polarized modes is very similar to the one of the longitudinal modes as it only differs for the slope and the bandwidth (not reported here). In this case, the branches of the pseudodispersion curve show a negative slope because the polarization parameter $\eta_\perp$ is positive. In summary, our calculations of the pseudodispersion diagrams of the dipolar modes in Fibonacci chains explain in very clear terms the origin of the plasmonic band-gap formation as d_B/d_A increases above the value of one.

C. Coupling with a uniform external electric field

Here we study the coupling of a linear Fibonacci chain with an external electric field $\mathbf{E}_0$ that is uniform and longitudinally polarized. The main features of the coupling are highlighted by studying the behavior of the electric-field enhancement and of the extinction cross sections.

The enhancement of the electric field is defined as the ratio between the amplitude of the induced electric field E and the amplitude of the external electric field E_0. We will denote with E_p the electric-field amplitude at the intermediate points between adjacent nanoparticles along the chain axis with abscissa $\bar{x}_p=(x_p+x_{p+1})/2$ where x_h denotes the abscissa of the center of the h-th particle and $p=1,2,\ldots,N-1$. We will consider the extinction cross section, normalized to the "geometrical" extinction cross section $C_{\text{ext}}^{(0)} \equiv V_0\omega_p/c$ where c denotes the light velocity in the vacuum. Here we will always refer to a Fibonacci chain with index $j=10$.

It is interesting to study the behavior of the maximum of the electric-field enhancement $\max_{p\in[1,N-1]}(E_p/E_0)$ along the chain axis. In Figs. 6(a)–6(d) we show $\max_{p\in[1,N-1]}(E_p/E_0)$ versus the resonance frequency Ω_m of the m-th mode, normalized to the plasma frequency, obtained by tuning $\mathbf{E}_0$ on Ω_m for several values of d_B/d_A. In Figs. 6(e) and 6(f) we show the participation ratios versus Ω_m for $d_B/d_A=1.25$ and $d_B/d_A=2$. For $d_B/d_A=1$ [Fig. 5(a)] the largest value of the enhancement is obtained by tuning $\mathbf{E}_0$ on $\Omega_1 \cong 0.542\omega_p$ and $\max_{p\in[1,N-1]}(E_p/E_0)$ decreases rapidly as Ω_m increases. Only the modes with index $m=1,3,\ldots$ couple significantly with the external source and the coupling coefficients tend to zero as the resonance frequency of the mode increases. We observed that the maximum enhancement of the modes with $\Omega_m > \Omega_{13} \cong 0.527\omega_p$ is less than 10^3. As d_B/d_A increases, the maximum enhancement of the modes for which $\Omega_1 \le \Omega_m \le \Omega_{55} \cong 0.556\omega_p$ rapidly increases, as shown in Figs. 6(b)–6(d). For $d_B/d_A=2$ [Fig. 6(d)] the maximum enhancement is of the order of 10^3 for $\Omega_1 \le \Omega_m \le \Omega_{55}$ and has four maxima: the absolute maximum at Ω_1 and three local maxima at $\Omega_{18} \cong 0.532\omega_p$, $\Omega_{34} \cong 0.546\omega_p$, and $\Omega_{43} \cong 0.554\omega_p$. The maximum enhancement also features several discontinuities. The largest discontinuities are around $\Omega_{22} \cong 0.544\omega_p$, Ω_{34}, and Ω_{55}. The enhancement reduces roughly

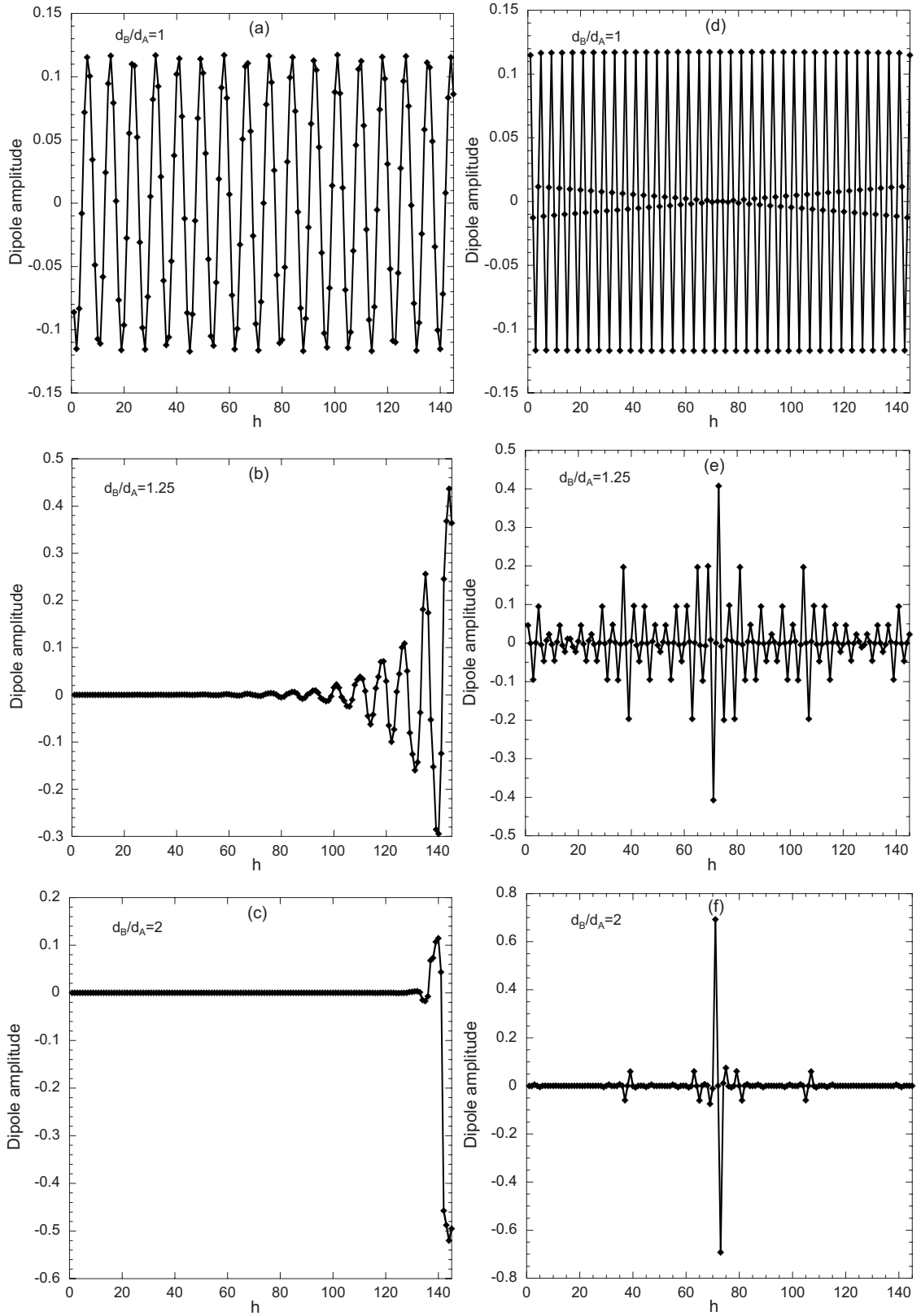

FIG. 4. Linear Fibonacci chain with $j=10$: distributions of the [(a)–(c)] 34-th mode ($\Omega_{34} \cong 0.553\omega_p$) and [(d)–(f)] 73-th mode ($\Omega_{73} \cong 0.580\omega_p$) for $d_B/d_A=1$, $d_B/d_A=1.25$, and $d_B/d_A=2$.

of a factor of 30 moving from Ω_{55} to $\Omega_{56} \cong 0.558\omega_p$. This is a consequence of the wide gap situated at Ω_{56} in the dispersion diagram [Fig. 1(c)] and of the low coupling of the uniform external source with the modes with resonance frequencies greater than Ω_{56}. The 34-th mode is one of the modes with the minimum participation ratio in the interval $1 \leq m$

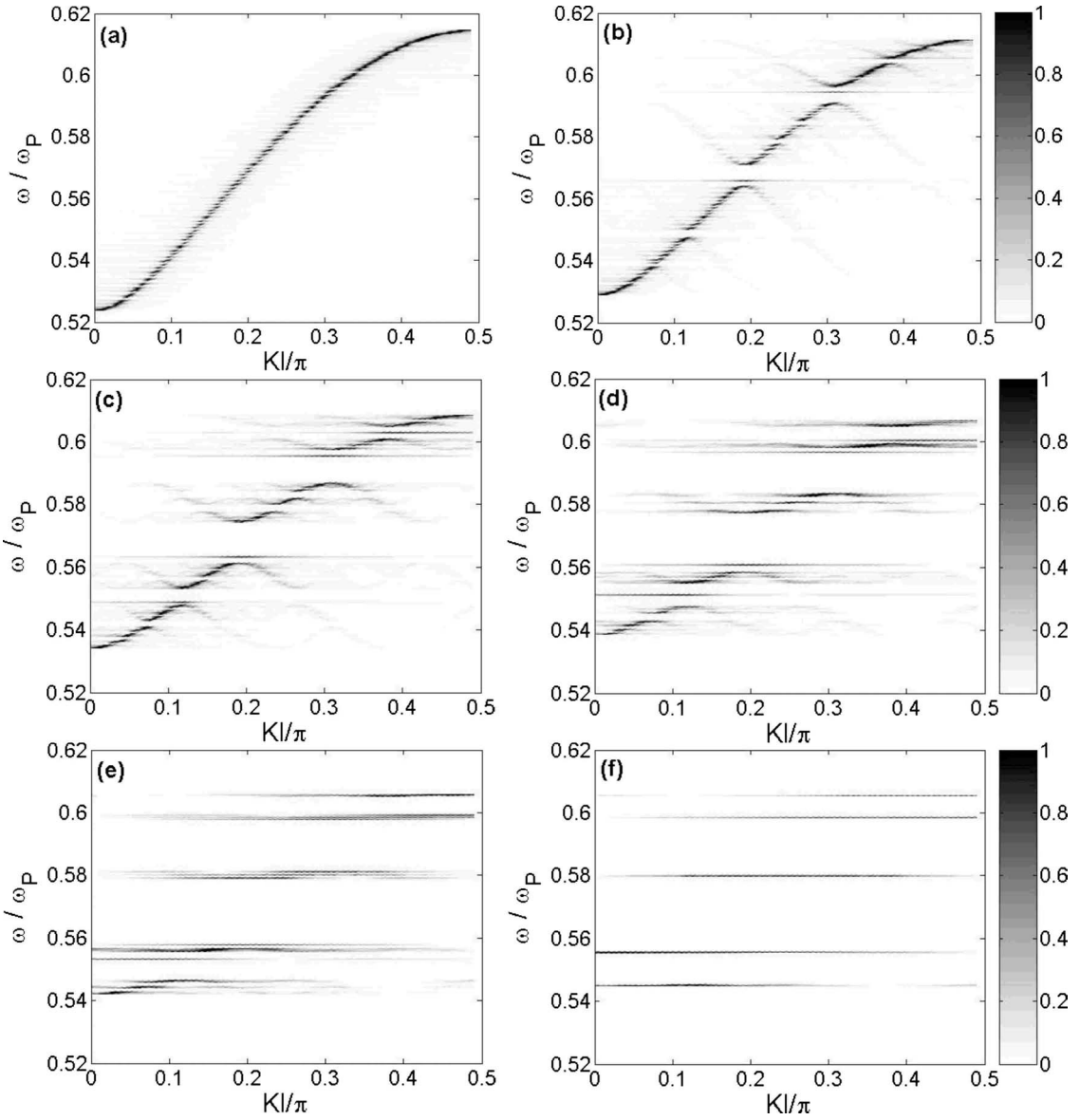

FIG. 5. Linear Fibonacci chain with $j=10$: pseudodispersion diagrams of the longitudinal modes for (a) $d_B/d_A=1$, (b) $d_B/d_A=1.1$, (c) $d_B/d_A=1.25$, (d) $d_B/d_A=1.5$, (e) $d_B/d_A=2$, and (f) $d_B/d_A=5$.

≤ 55, as shown in Figs. 6(e) and 6(f). Therefore an external electric field tuned on the resonance frequency of the 34-th may induce a dipole distribution that generates a strongly enhanced and localized electric field. However, it is important to notice that the electric-field enhancement corresponding to the second most localized mode in the Fibonacci chain (namely, the 73-th mode) is less than 100, clearly indicating that mode localization and field enhancement are not always correlated in aperiodic chains.

Figures 7 shows the distribution of the enhancement of the electric E_p/E_0 versus $\bar{x}_p/l$, induced by a uniform external electric field $\mathbf{E}_0$ tuned on the resonance frequency of the 34-th mode for $d_B/d_A=1$, $d_B/d_A=1.25$, and $d_B/d_A=2$. In the periodic case, an enhanced field extends along the interior part of the chain axis, as shown in Fig. 7(a). For $d_B/d_A=1.25$, differently from the periodic case, the enhancement is more localized on the right end side of the chain while for $d_B/d_A=2.0$ it becomes strongly localized. On the other hand, for values of d_B/d_A larger than four, many electric-field spots are distributed along the chain. This is due to the strong degeneracy of the system as we have seen before. In this case all the small clusters are individually excited at resonance with $\mathbf{E}_0$.

Figures 8(a) and 9(a) show $\max_{p\in[1,N-1]}(E_p/E_0)$ versus ω/ω_p for $d_B/d_A=1$ and $d_B/d_A=2.0$, respectively; Figs. 8(b) and 9(b) show the normalized extinction cross section versus ω/ω_p for the same cases. We notice that the maxima of $\max_{p\in[1,N-1]}(E_p/E_0)$ and $C_{\text{ext}}/C_{\text{ext}}^{(0)}$ occur for the same values of the frequency. For $d_B/d_A=1$ the curves $\max_{p\in[1,N-1]}(E_p/E_0)$ and $C_{\text{ext}}/C_{\text{ext}}^{(0)}$ have only one maximum at $\omega/\omega_p\cong 0.5235$, which is the resonance frequency of the 1-th mode. Unlike the periodic case, for $d_B/d_A=2.0$ both the curves have four peaks

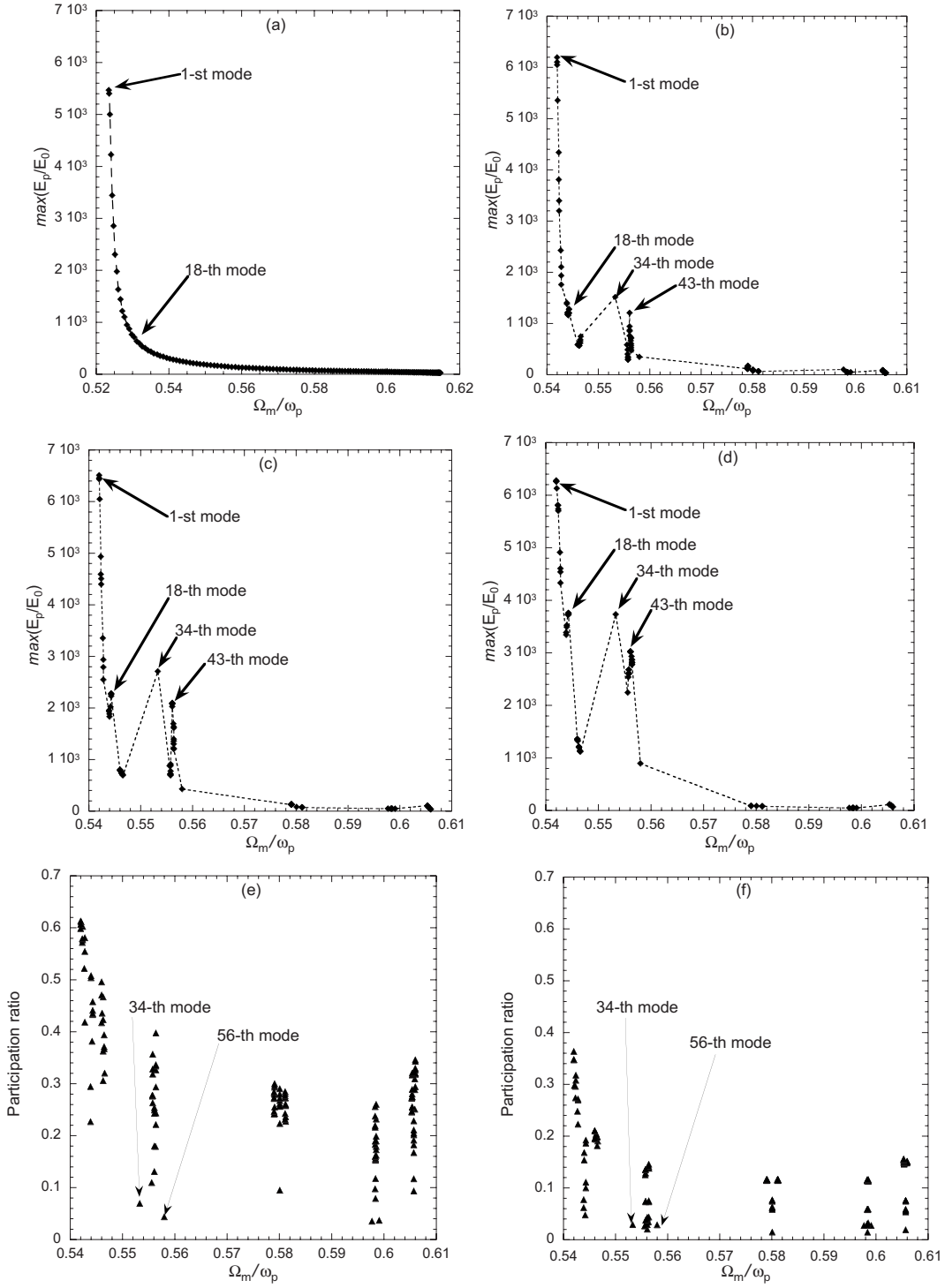

FIG. 6. Linear Fibonacci chain with $j=10$: maximum of the enhancement of the electric field $\max_{p\in[0,N-1]}(E_p/E_0)$ vs Ω_m/ω_p for $\mathbf{E}_0$ tuned on the resonant frequency of the m-th mode Ω_m for (a) $d_B/d_A=1$, (b) $d_B/d_A=1.25$, (c) $d_B/d_A=1.5$, and (d) $d_B/d_A=2$. Participation ratio vs the normalized mode resonance frequency Ω_m/ω_p for (e) $d_B/d_A=1.25$ and (f) $d_B/d_A=2$.

that correspond to the resonance frequencies of the modes for which $\max_{p\in[1,N-1]}(E_p/E_0)$ is maximum [see Fig. 9(b)]. In Figs. 9(a) and 9(b), the first peak (from the left) is the highest one, and occurs at the resonance frequency of the 1-th mode. The second peak occurs at the resonance frequency of the 18-th mode, the third peak occurs at the resonance frequency of the 34-th mode, and the fourth peak occurs at the resonance frequency of the 43-th mode. The depression between the 18-th and the 34-th modes, in both curves, is due to the gap at Ω_{34} in the dispersion diagram [Fig. 1(c)]. For frequencies greater than the resonance frequency of the 46-th mode, the enhancement and the extinction cross section falls to zero because of the gap at Ω_{56} in the dispersion diagram [Fig.

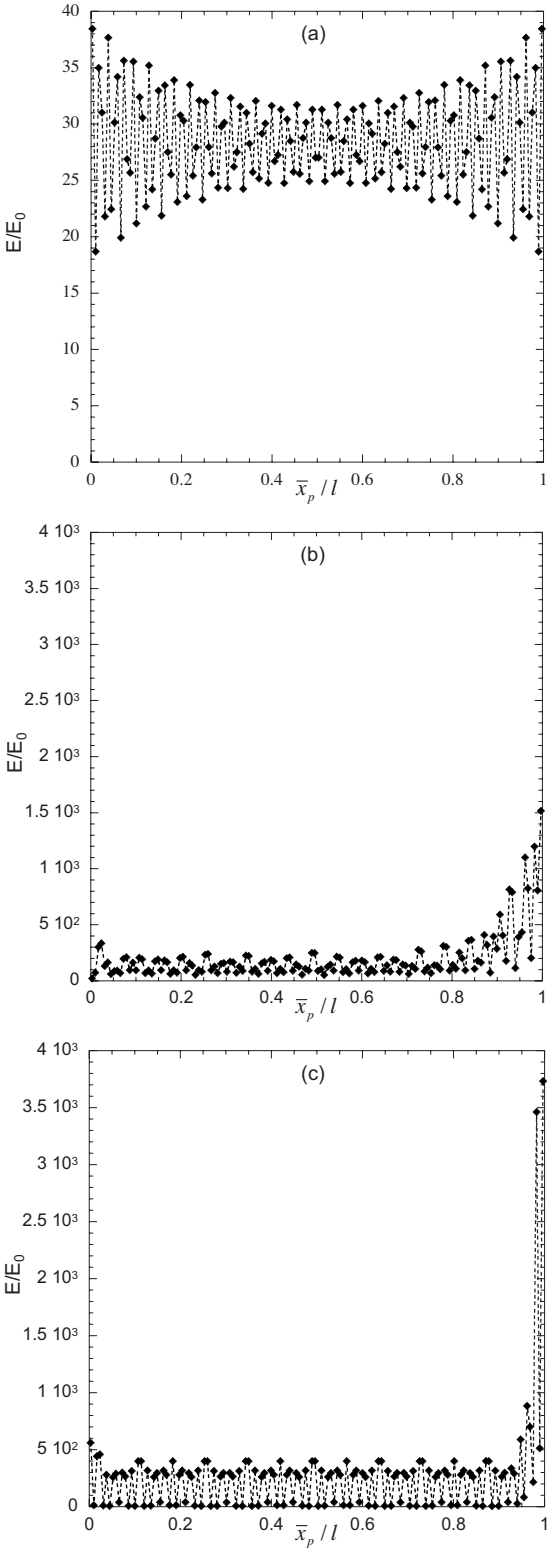

FIG. 7. Linear Fibonacci chain with $j=10$: electric-field enhancement E/E_0 vs $\bar{x}_p/l$ for $\mathbf{E}_0$ tuned on the resonance frequency of the 34-th mode $\Omega_{34}\cong 0.553\omega_p$ for (a) $d_B/d_A=1$, (b) $d_B/d_A=1.25$, and (c) $d_B/d_A=2$.

1(c)] and the weak coupling of the modes with $\Omega_m > \Omega_{56}$ with the external electric field. The losses affect dramatically the response of the chain to an applied electric field. The

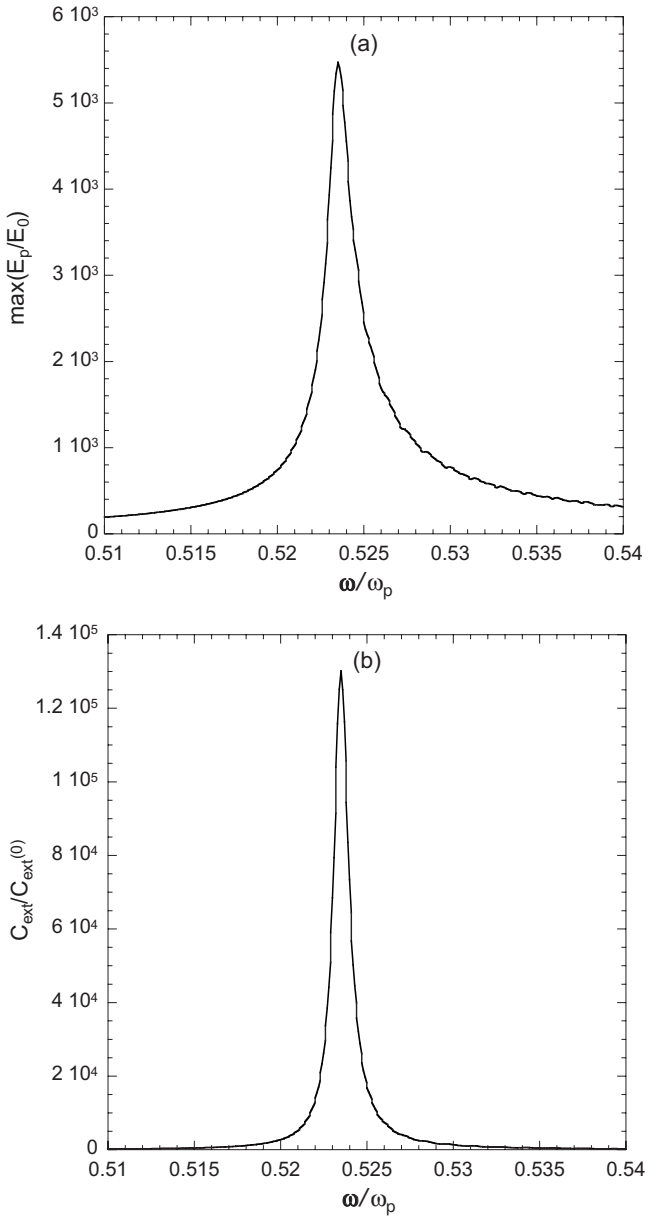

FIG. 8. Linear Fibonacci chain with $j=10$ and $d_B/d_A=1$: (a) $\max_{p\in[0,N-1]}(E_p/E_0)$ vs ω/ω_p; (b) extinction cross section vs ω/ω_p.

results discussed here have been obtained by assuming $\nu/\omega_p=10^{-3}$. As the quantity ν/ω_p increases the 3 dB band of the mode response functions also increases and it becomes more difficult to select localized modes. Indeed, as the effects of the losses increase, both the enhancement and the extinction cross-section curves tend to a curve with only one maximum.

By summarizing, electric fields with high amplitudes (thousand times the amplitude of the uniform external electric field) can be obtained and the maximum enhancement of the electric field along the chain axis first increases as the Fibonacci index increases for fixed d_B/d_A, then decreases slightly, and finally tends to a constant value.

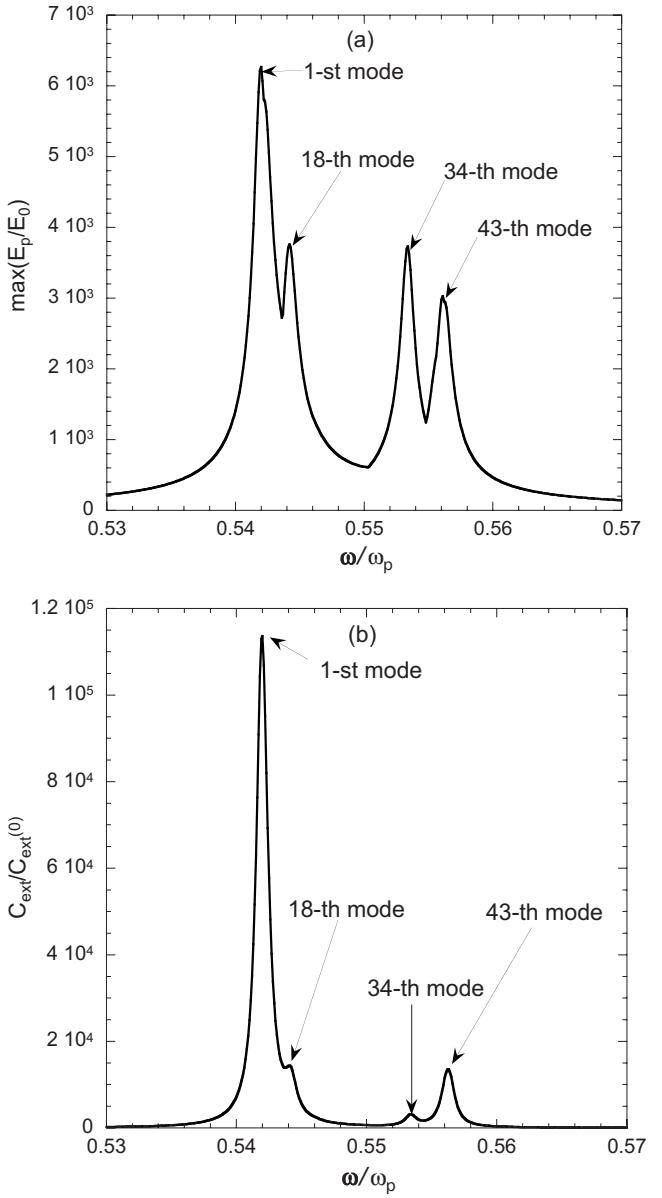

FIG. 9. Linear Fibonacci chain with $j=10$ and $d_B/d_A=2$: (a) $\max_{p\in[1,N-1]}(E_p/E_0)$ vs ω/ω_p; (b) extinction cross section vs ω/ω_p.

VI. CONCLUSIONS

We have proposed a simple and effective computational approach, based on the electric quasistatic approximation, to analyze both the dipolar modes of aperiodic deterministic arrays of metal nanoparticles and their coupling with an external electric field. The proposed approach has several significant advantages. A simple calculation yields the eigenfrequencies and plasmon modes of arbitrary chain geometry. Particles with ellipsoidal shape and arbitrary dielectric functions can be treated. The equations governing the plasmon oscillations are formulated in such a way as to clearly highlight the role of the geometrical arrangement of the particles on one side, and particle shape, dielectric response, and polarization on the other side. We have found a predictive and efficient way of calculating the plasmonic band-gap positions in general aperiodic chains, and we have clearly correlated the geometry of the aperiodic chains with the resulting spectral properties.

The method has been specifically applied to the case of a linear Fibonacci chain of metal nanoparticles. We have explained the origin and the mechanism of band-gap formation, and correlated their frequency positions with the spectral components of the Fibonacci chain. We have examined the behavior of the participation ratio and the localization properties of Fibonacci modes, and we have studied the coupling of the nanoparticle array with an external electric field. Finally we discussed the behavior of the electric-field enhancement and extinction cross sections of Fibonacci chains.

The results of our investigation demonstrate the potential of the proposed computational approach for the accurate design of aperiodic plasmonic devices. We believe that the possibility to accurately understand and predict the complex behavior of enhanced localized plasmon fields in resonant aperiodic environments can have a significant impact for the fabrication and optimization of active nanoplasmonic devices such as plasmonic sensors, compact nonlinear optical elements, and engineered substrates for surface enhanced Raman scattering (SERS) applications.

ACKNOWLEDGMENTS

This work was partially supported by the College of Engineering Dean's Catalyst Award at Boston University, the U.S. Army Research Laboratory under the Contracts No. W911NF-06-2-0040 and No. W911NF-07-1-0618, and the EURATOM/ENEA/CREATE Association.

APPENDIX A

The expression of the depolarization factor A_t is given by (e.g., Ref. 22)

$$A_t = \frac{a_x a_y a_z}{2}\int_0^\infty \frac{ds}{(s+a_t^2)\sqrt{(s+a_x^2)(s+a_y^2)(s+a_z^2)}} \quad \text{with} \quad t = x,y,z. \tag{A1}$$

The quantities A_x, A_y, A_z verify the properties:

$$A_x + A_y + A_z = 1, \tag{A2}$$

$$A_x \le A_y \le A_z. \tag{A3}$$

The integrals [Eq. (A1)] may be evaluated analytically in some notably cases: *prolate* spheroid, *oblate* spheroid, and sphere. For a sphere it is $A_x=A_y=A_z=1/3$. For a *prolate* spheroid $a_x=a_y$ (cigar shaped) it is $A_y=A_x$ and

$$A_z = \frac{1-e^2}{e^2}\left(-1+\frac{1}{2e}\ln\frac{1+e}{1-e}\right), \tag{A4}$$

where

$$e = \sqrt{1-\frac{a_x^2}{a_z^2}} \tag{A5}$$

is the eccentricity of the ellipsoid. The shape of the prolate

spheroid ranges from a *needle* ($e=1$, $A_z=0$) to a sphere ($e=0$, $A_z=1/3$). For an oblate spheroid $a_y=a_z$ (pancake shaped) it is $A_y=A_z$,

$$A_z = \frac{g(e)}{2e^2}\left[\frac{\pi}{2} - \tan^{-1} g(e)\right] - \frac{g^2(e)}{2}, \tag{A6}$$

where now

$$e = \sqrt{1 - \frac{a_z^2}{a_x^2}}, \tag{A7}$$

and

$$g(e) = \sqrt{\frac{1-e^2}{e^2}}. \tag{A8}$$

The shape of the *oblate* spheroid ranges from a *disk* ($e=1$, $A_z=0$) to a sphere ($e=0$, $A_z=1/3$). In both cases A_z varies in the interval (0,1/3) and tends monotonically to 0 as $e \to 1$.

[1] J. M. Luck, Phys. Rev. B **39**, 5834 (1989).
[2] M. Queffélec, *Substitution Dynamical Systems-Spectral Analysis*, Lecture Notes in Mathematics (Springer, Berlin, 1987), Vol. 1294.
[3] M. Dulea, M. Johansson, and R. Riklund, Phys. Rev. B **45**, 105 (1992).
[4] E. Macia, Rep. Prog. Phys. **69**, 397 (2006).
[5] *Symbolic dynamics and its applications*, edited by Susan G. Williams (American Mathematical Society, Providence, RI, 2004).
[6] J. Wolny, A. Wnek, and J. L. Verger-Gaugry, J. Comput. Phys. **163**, 313 (2000).
[7] A. Rudinger and F. Piechon, J. Phys. A **31**, 155 (1998).
[8] C. Godreche and J. M. Luck, J. Phys. A **23**, 3769 (1990).
[9] P. Prusinkiewicz and A. Lindenmayer, *The Algorithmic Beauty of Plants* (Springer, New York, 1990).
[10] M. Kohmoto, B. Sutherland, and C. Tang, Phys. Rev. B **35**, 1020 (1987).
[11] F. Iglòi, L. Turban, and H. Rieger, Phys. Rev. E. **59**, 1465 (1999).
[12] M. Dulea, M. Johansson, and R. Riklund, Phys. Rev. B. **45** 105 (1992).
[13] E. Maciá, Phys. Rev. B **60**, 10032 (1999).
[14] L. Dal Negro and N. N. Feng, Opt. Express **15** 14396 (2007).
[15] L. Dal Negro, N. N. Feng, and A. Gopinath, J. Opt. A, Pure Appl. Opt. **10**, 064013 (2008).
[16] A. Gopinath, S. Boriskina, N. N. Feng, B. M. Reinhard, and L. Dal Negro, Nano Lett. **8**, 2423 (2008).
[17] B. T. Draine and P. J. Flatau, J. Opt. Soc. Am. A Opt. Image Sci. Vis **11**, 1491 (1994).
[18] E. Purcell and C. R. Pennypacker, Astrophys. J. **186**, 705 (1973).
[19] B. T. Draine, Astrophys. J. **333**, 848 (1988).
[20] L. L. Zhao, K. L. Kelly, and G. C. Schatz, J. Phys. Chem. B **107**, 7343 (2003).
[21] L. Dal Negro, G. Miano, G. Rubinacci, A. Tamburrino, and S. Ventre, IEEE Trans. Magn. (to be published).
[22] C. F. Bohren and D. R. Huffman, *Absorption and scattering of Light by Small Particles* (Wiley-VCH, Weinheim, 1998).
[23] M. L. Brongersma, J. W. Hartman, and H. A. Atwater, Phys. Rev. B **62**, R16356 (2000).
[24] S. A. Maier, P. G. Kik, and H. A. Atwater, Phys. Rev. B **67**, 205402 (2003).
[25] L. Novotny and B. Hecht, *Principles of Nano-Optics* (Cambridge University Press, Cambridge, 2006).
[26] U. Kreibig and M. Vollmer, *Optical Properties Of Metal Clusters* (Springer-Verlag, New York, 1995).
[27] Rashid Zia, Jon A. Schuller, and Mark L. Brongersma, Mater. Today **9**, 20 (2006).
[28] G. H. Golub and C. F. Van Loan, *Matrix Computations* (Johns Hopkins University Press, Baltimore, MD, 1983).
[29] I. D. Mayergoyz, D. R. Friedkin, and Z. Zhang Phys. Rev. B **72**, 155412 (2005).
[30] C. Janot, *Quasicrystals: A Primer*, 2nd ed. (Oxford University Press, New York, 1997).
[31] A. Rudinger and F. Piechon, J. Phys. A **31**, 155 (1998).
[32] F. Craciun, A. Bettucci, E. Molinari, A. Petri, and A. Alippi, Phys. Rev. Lett. **68**, 1555 (1992).
[33] X. Fu, Y. Liu, B. Cheng, and D. Zheng, Phys. Rev. B **43**, 10808 (1991).
[34] Z. Cheng, R. Savit, and R. Merlin, Phys. Rev. B **37**, 4375 (1988).
[35] E. Liviotti, J. Phys.: Condens. Matter **8**, 5007 (1996).
[36] Marston Morse and G. A. Hedlund, Duke Math. J. **11**, 1 (1944).
[37] Marston Morse, Trans. Am. Math. Soc. **22**, 84 (1921).
[38] F. A. B. F. de Moura, L. P. Viana, and A. C. Frery, Phys. Rev. B **73**, 212302 (2006).